High-Pressure Melt Curve and Phase Diagram of Lithium

Mungo Frost, Jongjin B. Kim, Emma E. McBride, J. Ryan Peterson, Jesse S. Smith, Peihao Sun, and Siegfried H. Glenzer

The High-Pressure Melt Curve and Phase Diagram of Lithium

Mungo Frost,[1] Jongjin B. Kim,[1] Emma E. McBride,[1] J. Ryan Peterson,[1] Jesse S. Smith,[2] Peihao Sun,[1] and Siegfried H. Glenzer[1]

[1] *SLAC National Accelerator Laboratory, 2575 Sand Hill Road, Menlo Park, USA*

[2] *High Pressure Collaborative Access Team, X-ray Science Division, Argonne National Laboratory, Argonne, USA*

(Dated: July 12, 2019)

We investigate the phase diagram of lithium at temperatures of 200 K to 400 K, to pressures over 100 GPa using X-ray diffraction in diamond anvil cells, covering the region in which the melting curve is disputed. To overcome degradation of the diamond anvils by dense lithium we utilize a rapid compression scheme taking advantage of the high flux available at modern synchrotrons. Our results show the *hR1* and *cI16* phases to be stable to higher temperature than previously reported. The melting minima of lithium is found to be close to room temperature between 40 GPa and 60 GPa, below which the solid is crystalline. Analysis of the stability fields of the *cI16* and *oC88* phases suggest the existence of a triple point between these and an undetermined solid phase at 60 GPa between 220 K and 255 K.

The application of pressure transforms lithium from a prototypical simple metal to a complex system in which valence-core interactions cause a variety of remarkable behaviors. In recent years considerable experimental and theoretical effort has gone into understanding the structural properties and phase transitions of dense lithium. Theoretical studies have predicted a variety of low-coordination and low-symmetry structures, and electron localisation driven by increasing density [1–4]. At low temperatures, experiments have revealed remarkable changes in the nature of lithium including superconductivity [5, 6], metal-to-semiconductor transitions [7] and the observation of highly complex low symmetry phases with up to 88 atoms per unit cell [8]. Even the ground state of lithium at zero pressure was unknown until a recent study showed it to be *fcc*; the previously reported *9R* phase was determined to be a metastable, partially disordered, state [9, 10].

At ambient conditions lithium is a *bcc* metal. This transforms to *fcc* at 7.5 GPa at 298 K [11, 12]. When cooled and further compressed this was found to undergo transitions to the lower symmetry *hR1* and *cI16* phases at 39 GPa and 42 GPa, respectively, at 180 K [13]. At higher pressures the low temperature phase diagram of lithium was greatly extended with the discovery of the extremely complex *oC88*, *oC40* and *oC24* phases to 120 GPa [8].

The melting curve of lithium is known to have a maxima around 550 K and 10 GPa [14, 15]. All the alkali metals have a local maximum in their melting curves followed by a pronounced minimum at higher pressures [16–18]. This minimum is accompanied by the onset of complex, low symmetry phases [19, 20]. Such low symmetry phases have been observed in lithium [8], but the temperature of the melting minimum and role of quantum effects therein remain disputed [8, 14, 21–23].

There is a lack of experimental data on lithium at high *P-T* conditions due to the difficulties associated with its containment [15]. In diamond cell studies this is partic-ularly problematic at temperatures above 200 K where lithium degrades the diamond anvils at pressures greater than about 20 GPa [11, 12, 14]. As such, only two studies claim to have experimentally determined the location of the melting minimum of lithium. The first, by Guillaume *et al.*, [8] finds the minimum to be at 190 K between 40 GPa and 60 GPa by observing loss of X-ray diffraction indicative of loss of crystallinity. Such temperature conditions are low enough to significantly extend the lifespan of diamond anvils in contact with dense lithium. A later study [14] used lithium fluoride or alumina to protect the diamond anvils and found the melting minimum to be at 306 K and 44 GPa by resistivity measurements. They suggest the discrepancy could be resolved if the lithium below the melting curve were in an amorphous state.

The melting curve of lithium has also been investigated by first-principals theoretical studies. Tamblyn *et al.* [21] finds a minimum between 250 K and 300 K at 65 GPa, while Hernández et al. [22] finds the slope remains negative to 50 GPa where they report a melting temperature of 270 K. Both are in closer agreement with the experimental results obtained via resistivity measurements [14]. However, Elatresh *et al.* [23] find much closer agreement with the melting curve of Guillaume *et al.* with melting predicted around 200 K between 40 GPa and 60 GPa when quantum corrections are included.

In this study, we take advantage of the high X-ray flux available at modern synchrotrons to allow faster compression than is traditional in diamond anvil cell studies. This allowed the experiment to be conducted on a shorter timescale than that of lithium induced diamond anvil failure, and so X-ray diffraction on dense lithium could be performed to higher *P-T* conditions than previously achieved. It is likely that this method will be useful in the study of other materials which are damaging to diamond anvils under extreme conditions.

Lithium was compressed isothermally from around 15 GPa to anvil failure at 220 K, 255 K, 275 K, 320 K, 360 K, and 400 K at a rate of 0.2 to 1 GPa s^{-1}. Melting
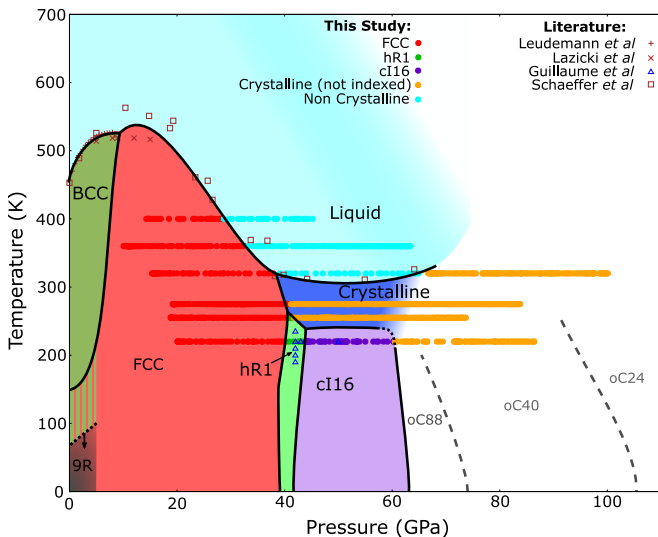
FIG. 1. Phase diagram of lithium. Filled circles show data points collected in this study, with orange circles indicating crystallinity, evidenced by Bragg diffraction, but with inconclusive indexing. Crosses and open symbols show melting points determined by other studies. Phase boundaries marked with solid lines take into account data from both this and other studies [8, 10–15, 18, 24, 25]. Grey dashed lines for the *oC88*, *oC40* and *oC24* phases are from ref. [8]. The dotted boundary of *cI16* near 60 GPa and 230 K indicates the probable location of a triple point, with an uncharacterised phase between *cI16* and the melt in blue. On isobaric cooling at low pressure the *bcc* to *fcc* transition does not occur, instead the metastable *9R* state forms from *bcc*-lithium at lower temperature, as indicated by the striped region and black dotted line [10]. All boundaries below 50 K are extrapolated.

was determined by the abrupt loss of diffraction peaks upon compression. Recrystallization was observed at 67 GPa in the 320 K run, indicated by the abrupt reemergence of diffraction peaks. We observe no evidence of melting at or below 275 K. Indeed, in the region of *P-T* space where melting has been previously reported by this criteria [8] we unambiguously find *hR1* and *cI16* lithium, with both phases being found to be stable to higher temperatures than previously reported. A phase diagram taking into account our new observations, as well as data from other studies, is shown in Figure 1.

High pressures were generated using diamond anvil cells equipped with Boehler-Almax type anvils [26] with 150 μm culets beveled to 300 μm at 8°. Rhenium gaskets of 250 μm initial thickness were pre-indented to ∼16 μm and 80 μm sample holes were cut using both laser drilling and electrical discharge machining.

Lithium of natural isotopic composition (99.9 % purity, Alfa Aesar) was loaded in a high purity argon atmosphere. A few flakes of powdered tungsten were added as a pressure marker as this is known not to react with lithium at pressures below 36 GPa [12]. We observe no indication of reactivity at higher pressures in this study.
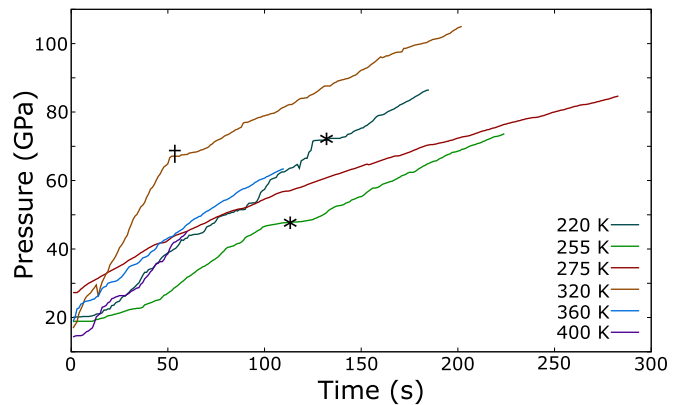

FIG. 2. Pressure vs time for the six runs. Stars indicate where compression was paused to realign the sample, the dagger indicates where the rate of pressure increase on the membrane was dropped during the 320 K run. The much higher compression rate than is customary leads to a much shorter experimental duration and allows data to be collected before the lithium degrades the diamond anvils.

The very small quantity of tungsten persisted to the highest pressures and the measured structures and volumes of lithium at lower pressure agree with existing literature; except where expressly noted, for example the higher temperature stability of the *hR1* phase. The pressure was determined via the equation of state of tungsten [27]. X-ray diffraction was performed at Advanced Photon Source (APS) HP-CAT ID-B using 0.4066 Å radiation.

Samples were cooled using a cryostat or heated using an external resistive ring heater. Temperatures were measured with a band B1 silicon diode below room temperature and a type K thermocouple above. In both cases the temperature uncertainty is 2 K. Force was applied to the cells using a gas membrane. Initially the cells were statically pre-compressed to between 15 GPa and 20 GPa before pressure was rapidly ramped at between 0.2 and 1 GPa s^{-1} until anvil failure. A plot of pressure vs time is shown in Figure 2. Typically, both anvils failed catastrophically, but three where recovered with only superficial cracks. Inspection of these under a polarising microscope revealed no evidence of lithium damage to the culets. Data were collected continually using a Pilatus 1MF detector with 995 ms exposures at 1 Hz. In all cases at low pressure, where it is well understood, the lithium showed no evidence of contamination and followed the established phase progressions. Runs were terminated if contamination was detected or when pressure dropped with increasing membrane load indicating anvil failure.

Lithium scatters X-rays very weakly making data analysis challenging. This is exacerbated by the necessarily short collection times needed to overcome lithium degradation of the anvils using the rapid compression technique employed here. At high pressure the quality

of the powder deteriorates, particularly at phase transitions, and ultimately the lithium forms single, or very few, crystals with isolated diffraction spots rather than rings. These are extremely weak and difficult to distinguish from other features, for example scattering from beamline components, cryostat windows and detector artefacts.

To overcome the weak signal, individual frames of the diffraction patterns were combined and then earlier frames collected at slightly lower pressure were used as a background subtraction. The total number of frames collected varied from 60 to 300 depending on the duration of the run, see Figure 2. To extract the signal arising from lithium, frames n to $n + 4$ are summed and frames $n - 9$ to $n - 5$ subtracted. This accounts for changes in the cell background with increasing pressure. It also allows determination of which features arise from the lithium sample as the angle of diffraction from these will monotonically increase with pressure. In this way, extremely weak reflections from lithium could still be fitted while features not due to the lithium sample could be rejected. It is possible that features from lithium coinciding with reflections from the tungsten pressure marker and rhenium gasket would not be detectable, however the difference in their compressibilities means that the overlap would only persist over a small pressure range.

Compressions were performed at 220 K, 255 K, 275 K, 320 K, 360 K, and 400 K, as shown in Figure 1. These effectively cover the disputed region of the phase diagram where there is little structural data available. The *hR1* phase is observed to be stable to higher temperature than previously reported [8] with an upper temperature limit of stability between 255 K and 275 K at 41 GPa. Additionally we observe *cI16* lithium between 44 GPa and 60 GPa at 220 K, a higher temperature than has been previously observed, refining its upper temperature boundary. Integrated patterns and fits of both phases are shown in Figure 3, along with *P-V* data for *cI16* lithium. This is fitted to a Vinet equation of state with $B_0 = 14.0(7)$ GPa and $B_0' = 2.99(13)$ for V_0 fixed at the zero pressure *bcc* value of $21.6225\,\text{Å}^3$. These values are similar to other equations of state and *P-V* data for lithium [8, 11, 12].

At higher pressures, cryogenic lithium adopts a variety of complex structures which have been investigated using single crystal diffraction [8]. Even with rapid compression employed in this study the samples formed single (or very few) crystals at higher pressure. However, the much longer times required to rotate the sample in the X-ray beam to collect a single crystal dataset would result in anvil failure due to lithium attack and are not possible in conjunction with rapid compression. As a result, only a limited subset of the reflections which occur at the particular angle the crystal formed with respect to the incident beam are observed. The diffraction spots can be traced as a function of pressure, as shown in Fig-
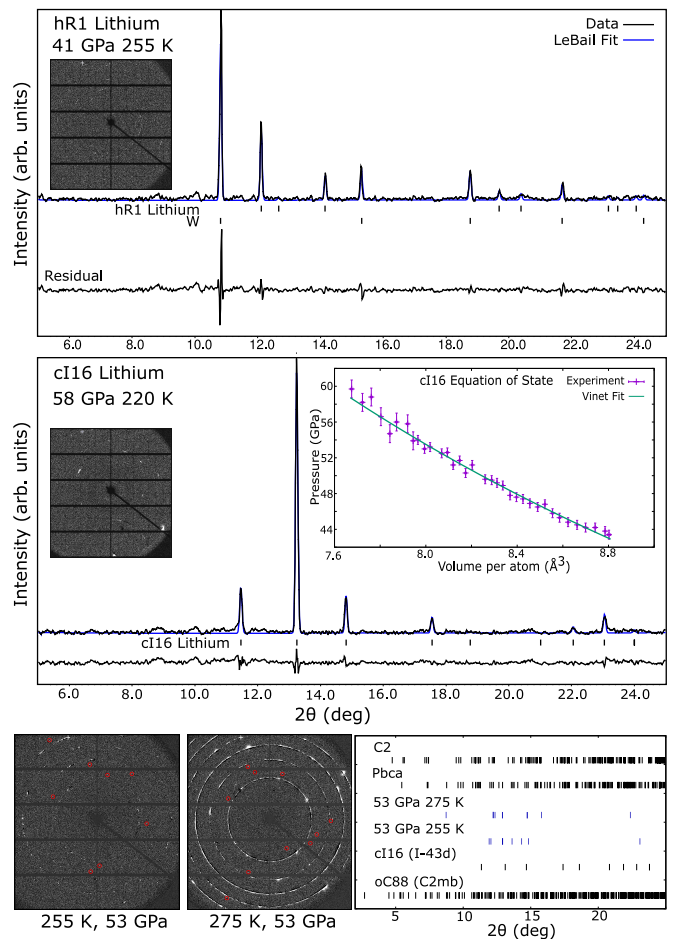

FIG. 3. *Top:* integrated powder pattern of *hR1* lithium at 255 K and 44 GPa. Data (black) with LeBail fit (blue) and residual (below). Tics indicate possible *hR1* and tungsten peaks as marked. The unintegrated pattern (inset) is the difference of five frames before and after transformation to the higher pressure phase with negative values suppressed. *Middle:* a similar plot for *cI16* lithium. Diamond and tungsten peaks were masked before integration. Additional inset shows pressure vs volume data for *cI16* lithium. *Bottom, left and centre:* Patterns prepared as above at 53 GPa in the region between *cI16* and the melt, red circles indicate lithium diffraction. *Right:* angles of observed peaks and the possible reflections of various phases. Reflections observed are not compatible with *cI16*, while *oC88* has a very large number of potential reflections which makes indexing ambiguous. Two candidates from theoretical studies, *C2* [4, 28] and *Pbca* [3, 4] are also shown. *Pbca* shows the best fit of all structures tried. X-ray diffraction was carried out using 0.4066 Å radiation.

ure 4. To distinguish the very weak features arising from the compressed lithium from artefacts successive frames were compared as described above and only those reflections which appeared on successive frames, and which increased in diffracted angle under compression are considered. Further those arising from non-sample cell components such as the gasket and pressure marker are omitted for clarity.
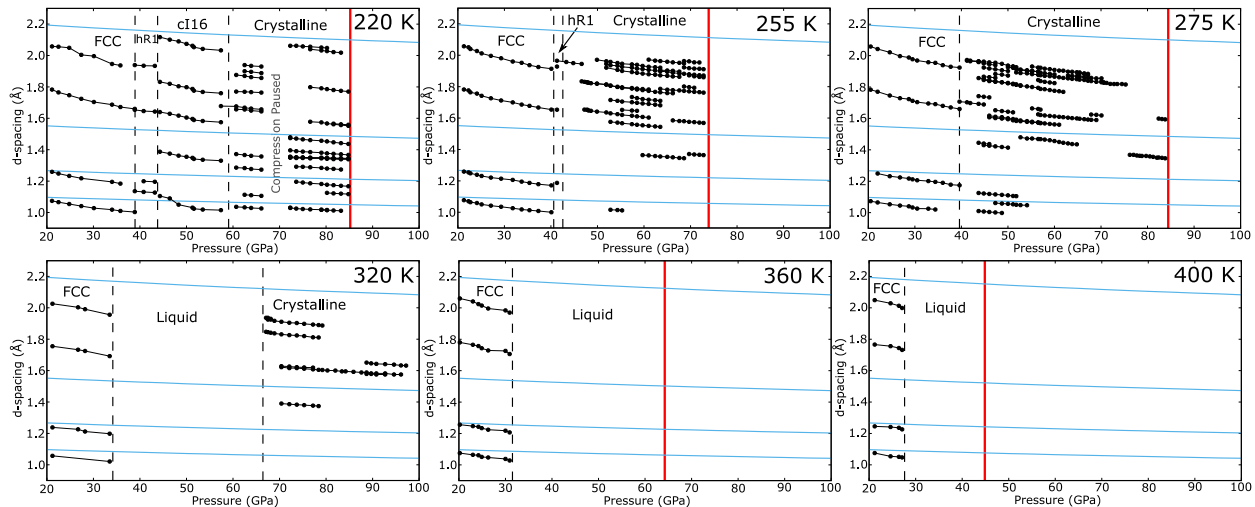
FIG. 4. Observed d-spacings of diffraction peaks between 0.9 Å and 2.3 Å from high pressure lithium. Lines linking points imply that they occur at the same detector location shot to shot and are identified as the same reflection. Pale blue lines indicate the first four diffraction lines of tungsten [27]. Red vertical lines indicate maximum pressure of a run. Data for higher d-spacings are presented in the supplemental materials.

The presence of Bragg diffraction shows that the lithium is crystalline under these conditions. However, the data are not sufficient to unambiguously assign a structure. In all cases the observed peaks are compatible with the known [8] *oC88* or *oC40* depending on pressure, though it should be noted that these low symmetry structures with large unit cells have a great many possible reflections which make such a fit inconclusive.

The observation of crystalline lithium in the region between 40 GPa and 60 GPa between 220 K and 275 K disagrees with the prior X-ray diffraction study in this region [8] which reports loss of diffraction around 45 GPa and 220 K. Under these conditions the *hR1* and *cI16* phases are observed here. Observation of crystalline diffraction also excludes an amorphous state below the melt. A possible explanation for the discrepancy is that of the *P-T* path followed. It is known that the phase adopted by lithium is *P-T* path dependent and that it can form disordered metastable states at low temperature [10]. One prior melting study observed slow recrystalization in this regime [14].

It is also noteworthy that the peaks observed at pressures beyond the *hR1* and *fcc* phases at 255 K and 275 K, respectively, are not compatible with *cI16* lithium, see Figure 3. This suggests that a different phase is favored by temperature and *cI16* does not border the melt as was previously assumed [8, 21, 22]. Combined with prior data on the *cI16* to *oC88* transition at low temperature [8, 24] there appears to be a rather sharp angle in stability field of *cI16* lithium indicative of a triple point near 60 GPa, see Figure 1. If this is the case, it implies that the intermediate phase between *cI16* and the melt is not

oC88 and is a new, uncharacterised, phase of lithium. The angles of the observed peaks at 53 GPa and 255 K and 275 K, as well as those of *cI16*, *oC88* and two phases predicted by theory, *C2* [4, 28] and *Pbca* [3, 4] are shown in Figure 3.

At a temperature of 320 K, melting is detected from the *fcc* phase at 38 GPa by the abrupt loss of diffraction from the sample. Effort was made to extract liquid diffraction signal but, not unexpectedly, it is too weak to be distinguished from the background. On compression of the liquid, recrystallization is observed at 67 GPa indicating the melting curve has a positive slope by this pressure. As with the low temperature runs this forms a single crystal. The observed peaks are shown in Figure 4, and may be fitted to either the *oC88* or *oC40* phases known experimentally [8]. They are also compatible with the *C2* phase predicted by theory [4, 28]. Compression at 360 K and 400 K resulted in the sudden loss of *fcc* diffraction at 32 GPa and 28 GPa, respectively. Recrystallization was not observed below the maximum pressures in either run.

The melting curve of lithium is shown in Figure 1, along with points from other studies. It has a minimum between 275 K and 320 K. This is in far better agreement with the melt curve reported via resistivity measurements [14] than those of the previous diffraction study [8]. No evidence of an amorphous phase is observed below the melting curve on isothermal compression. The melting curve has also been approached theoretically using first principles molecular dynamics simulations. Tamblyn *et al.* [21] find a qualitatively similar minimum to that reported here, though at somewhat higher pressures. The melting curve of Hernández *et al.* [22] is very close to that

reported here below 40 GPa, though the suggested conversion from *fcc* to *bcc* prior to melting is not observed. Elatresh *et al.* predict lower melting temperatures between 40 GPa and 60 GPa than are measured here.

The success of compressing rapidly to overcome lithium degradation of the anvils is striking and has allowed X-ray diffraction data to be collected at higher pressures and temperatures than is possible with traditional methods. Indeed, to the authors' knowledge no high temperature diffraction has previously been performed on lithium in a diamond anvil cell. The advent of X-ray free electron lasers [29] offers particular promise for this technique, as their increased flux and pulsed nature are ideally suited to pushing for even higher compression rates. This is a promising route to explore the lithium melt curve and high-temperature phases in the megabar regime.

In conclusion we have demonstrated that fast compression allows lithium to be studied under conditions previously prohibited by diamond anvil degradation. Isothermal compression to high pressures was performed at various temperatures between 220 K and 400 K investigating the disputed melting region. An updated phase diagram is presented revealing the *hR1* and *cI16* phases to be stable to higher temperatures than previously thought. The melt curve is found to have a minimum between 275 K and 320 K around 50 GPa with no 'cold melting' or amorphous solid below the melt curve under the conditions and *P-T* paths studied. The melting curve results and suggested triple point above 220 K at 60 GPa will serve as a test and motivation for theoretical investigations.

[1] J. Neaton and N. Ashcroft, Nature **400**, 141 (1999).

[2] M. Marqués, M. McMahon, E. Gregoryanz, M. Hanfland, C. Guillaume, C. Pickard, G. Ackland, and R. Nelmes, Physical Review Letters **106**, 095502 (2011).

[3] C. J. Pickard and R. Needs, Physical Review Letters **102**, 146401 (2009).

[4] J. Lv, Y. Wang, L. Zhu, and Y. Ma, Physical Review Letters **106**, 015503 (2011).

[5] K. Shimizu, H. Ishikawa, D. Takao, T. Yagi, and K. Amaya, Nature **419**, 597 (2002).

[6] V. V. Struzhkin, M. I. Eremets, W. Gan, H.-k. Mao, and R. J. Hemley, Science **298**, 1213 (2002).

[7] T. Matsuoka and K. Shimizu, Nature **458**, 186 (2009).

[8] C. L. Guillaume, E. Gregoryanz, O. Degtyareva, M. I. McMahon, M. Hanfland, S. Evans, M. Guthrie, S. V. Sinogeikin, and H. Mao, Nature Physics **7**, 211 (2011).

[9] A. Overhauser, Physical review letters **53**, 64 (1984).

[10] G. J. Ackland, M. Dunuwille, M. Martinez-Canales, I. Loa, R. Zhang, S. Sinogeikin, W. Cai, and S. Deemyad, Science **356**, 1254 (2017).

[11] M. Hanfland, I. Loa, K. Syassen, U. Schwarz, and K. Takemura, Solid state communications **112**, 123 (1999).

[12] M. Frost, A. L. Levitan, P. Sun, and S. Glenzer, Journal of Applied Physics **123**, 065901 (2018).

[13] M. Hanfland, K. Syassen, N. Christensen, and D. Novikov, Nature **408**, 174 (2000).

[14] A. M. J. Schaeffer, W. B. Talmadge, S. R. Temple, and S. Deemyad, Physical Review Letters **109**, 185702 (2012).

[15] A. Lazicki, Y. Fei, and R. J. Hemley, Solid State Communications **150**, 625 (2010).

[16] E. Gregoryanz, O. Degtyareva, M. Somayazulu, R. J. Hemley, and H.-k. Mao, Physical Review Letters **94**, 185502 (2005).

[17] E. E. McBride, K. A. Munro, G. W. Stinton, R. J. Husband, R. Briggs, H.-P. Liermann, and M. I. McMahon, Physical Review B **91**, 144111 (2015).

[18] H. Luedemann and G. Kennedy, Journal of Geophysical Research **73**, 2795 (1968).

[19] M. Hanfland, I. Loa, and K. Syassen, Physical Review B **65**, 184109 (2002).

[20] H. Olijnyk and W. Holzapfel, Physics Letters A **99**, 381 (1983).

[21] I. Tamblyn, J.-Y. Raty, and S. A. Bonev, Physical Review Letters **101**, 075703 (2008).

[22] E. R. Hernández, A. Rodriguez-Prieto, A. Bergara, and D. Alfe, Physical Review Letters **104**, 185701 (2010).

[23] S. Elatresh, S. Bonev, E. Gregoryanz, and N. Ashcroft, Physical Review B **94**, 104107 (2016).

[24] T. Matsuoka, M. Sakata, Y. Nakamoto, K. Takahama, K. Ichimaru, K. Mukai, K. Ohta, N. Hirao, Y. Ohishi, and K. Shimizu, Physical Review B **89**, 144103 (2014).

[25] V. Vaks, M. Katsnelson, V. Koreshkov, A. Likhtenstein, O. Parfenov, V. Skok, V. Sukhoparov, A. Trefilov, and A. Chernyshov, Journal of Physics: Condensed Matter **1**, 5319 (1989).

[26] R. Boehler and K. De Hantsetters, High Pressure Research **24**, 391 (2004).

[27] A. Dewaele, P. Loubeyre, and M. Mezouar, Physical Review B **70**, 094112 (2004).

[28] Y. Yao, S. T. John, and D. D. Klug, Physical Review Letters **102**, 115503 (2009).

[29] L. Fletcher, H. Lee, T. Döppner, E. Galtier, B. Nagler, P. Heimann, C. Fortmann, S. LePape, T. Ma, M. Millot, *et al.*, Nature photonics **9**, 274 (2015).